Received: 18 April 2021 | Revised: 31 August 2021 | Accepted: 8 October 2021

DOI: 10.1002/jev2.12162

RESEARCH ARTICLE

The impact of storage on extracellular vesicles: A systematic study

Stefano Gelibter[1] | **Giulia Marostica**[1] | **Alessandra Mandelli**[1] | **Stella Siciliani**[3] | **Paola Podini**[2] | **Annamaria Finardi**[1] | **Roberto Furlan**[1]

[1] Clinical Neuroimmunology Unit, Institute of Experimental Neurology, Division of Neuroscience, IRCCS Ospedale San Raffaele, Milan, Italy

[2] Neuropathology Unit, Institute of Experimental Neurology, Division of Neuroscience, IRCCS Ospedale San Raffaele, Milan, Italy

[3] Neuroimmunology Unit, Institute of Experimental Neurology, Division of Neuroscience, IRCCS Ospedale San Raffaele, Milan, Italy

Correspondence
Roberto Furlan, Clinical Neuroimmunology Unit, Institute of Experimental Neurology, Division of Neuroscience, IRCCS Ospedale San Raffaele Milan, Italy.
Email: furlan.roberto@hsr.it

Stefano Gelibter and Giulia Marostica are equally contributing first authors.

Please cite the paper as "Gelibter, Marostica et al".

Funding information
Italian Ministry of Health, Grant/Award Number: # RCR-2019-23669119_004

Abstract

Mounting evidence suggests that storage has an impact on extracellular vesicles (EVs) properties. While −80°C storage is a widespread approach, some authors proposed improved storage strategies with conflicting results. Here, we designed a systematic study to assess the impact of −80°C storage and freeze-thaw cycles on EVs. We tested the differences among eight storage strategies and investigated the possible fusion phenomena occurring during storage. EVs were collected from human plasma and murine microglia culture by size exclusion chromatography and ultracentrifugation, respectively. The analysis included: concentration, size and zeta potential (tunable resistive pulse sensing), contaminant protein assessment; flow cytometry for the analysis of two single fluorescent-tagged EVs populations (GFP and mCherry), mixed before preservation. We found that −80°C storage reduces EVs concentration and sample purity in a time-dependent manner. Furthermore, it increases the particle size and size variability and modifies EVs zeta potential, with a shift of EVs in size-charge plots. None of the tested conditions prevented the observed effects. Freeze-thaw cycles lead to an EVs reduction after the first cycle and to a cycle-dependent increase in particle size. With flow cytometry, after storage, we observed a significant population of double-positive EVs (GFP^+-$mCherry^+$). This observation may suggest the occurrence of fusion phenomena during storage. Our findings show a significant impact of storage on EVs samples in terms of particle loss, purity reduction and fusion phenomena leading to artefactual particles. Depending on downstream analyses and experimental settings, EVs should probably be processed from fresh, non-archival, samples in majority of cases.

KEYWORDS
extracellular vesicles, flow cytometry, fusion, preservation, size exclusion chromatography, storage, tunable resistive pulse sensing

1 | INTRODUCTION

Despite the great interest and the increasing number of studies addressing extracellular vesicles (EVs) in all medical and biological fields, challenges in EVs isolation, characterization and storage are still open and an important lack of standard procedures still remains (Marostica et al., 2021).

Concerning the preservation of the samples, mounting evidence suggests an impact of storage on EVs concentration, physical properties and functionality (Jeyaram & Jay, 2018; Kusuma et al., 2018). Both the storage of freshly isolated EVs and the recovery of EVs from previously-stored biological samples appear to affect the properties of the particles (Jeyaram & Jay, 2018). In 2013, the International Society for Extracellular Vesicles (ISEV) recommended preserving the samples at −80°C, further specifying to store

EVs in phosphate-buffered saline (PBS) in siliconized vessels (Witwer et al., 2013). In the 2018 update of ISEV guidelines, however, standard indications for biological samples or EVs storage were not provided anymore (Théry et al., 2018). These guidelines, recognizing the impact of preservation on EVs and their matrix, suggest to clearly describe the precise storage strategies and promote further investigations to better clarify the effect of storage and retrieval.

In the last years, few studies were focused on the effect of storage on EVs. These studies demonstrated that the storage method can impact EVs yield, physical properties and functionality (Jeyaram & Jay, 2018; Kusuma et al., 2018). Some authors propose the use of cryoprotective agents (CPA) such as trehalose (Bosch et al., 2016; Charoenviriyakul et al., 2018) or dimethyl sulfoxide (DMSO) (Tegegn et al., 2016; Wu et al., 2015), with promising results. A couple of studies suggested the use of lyophilization (Bosch et al., 2016; Charoenviriyakul et al., 2018), while others focused on the effect of different temperatures (Cheng et al., 2019; Issman et al., 2013; Lee et al., 2016; Lőrincz et al., 2014; Maroto et al., 2017; Park et al., 2018) or on the rapidity of freezing or thawing cycles (Bosch et al., 2016; Cheng et al., 2019; Trummer et al., 2009). Despite encouraging findings, some results are conflicting (Jeyaram & Jay, 2018; Kusuma et al., 2018; Qin et al., 2020) and systematic studies comparing different storage strategies at the same time are still lacking. Besides, most of these studies analysed samples after a relatively short time period (e.g., hours, days, seldom weeks) (Jeyaram & Jay, 2018) and those who analysed the samples after longer preservation periods mostly addressed the storage of biofluid samples instead of isolated EVs (Jeyaram & Jay, 2018; Welch et al., 2017).

In light of this lack of standard procedures, it should be advisable to work with fresh samples and to analyse EVs immediately after the collection of biological fluids and their isolation (Witwer et al., 2013). However, the storage could allow simultaneous analysis of samples from different sources or patients (Witwer et al., 2013). It could also allow working on previously biobanked samples (Witwer et al., 2013).

Against this background, the present study aims at systematically characterizing and comparing EVs populations taking into account different preservation strategies and timepoints, comparing them with fresh samples and investigating the phenomena occurring to particles during storage. By shedding more light on the impact of storage on EVs, we aim at contributing to reduce the pre-analytical variability in this research field.

2 | MATERIALS AND METHODS

2.1 | Study design

In order to compare freshly isolated EVs samples with samples stored in different conditions, we designed three sets of experiments.

The first experimental set was designed as depicted in Figure S1. At least 8 mL of purified platelet-free plasma (pPFP, see next section) were obtained from the human blood of five healthy donors (two females, mean age 28.8 years). 4 mL of pPFP were immediately used for EVs isolation. An aliquot of the fresh EVs sample (Fresh EVs - FE) was freshly analysed (particle concentration and size, contaminant protein concentration, zeta potential with tunable resistive pulse sensing–TRPS; transmission electron microscopy–TEM–imaging and immunogold labelling, western blot–WB). FE samples were then aliquoted into 16 tubes, two aliquots for each of the eight different storage conditions (Figure S1A). The samples were then stored in eight different conditions (see storage conditions). The other 4 mL of pPFP were immediately divided into 16 aliquots, two for each of the eight different storage conditions (Figure S1B). After 4 weeks of storage one aliquot of isolated EVs for each of the eight conditions was retrieved and analysed. The other aliquot for each of the eight conditions was analysed after 6 months of storage (Figure S1A). At the same time points, an aliquot of pPFP for each of the eight conditions was retrieved. EVs were then isolated from each aliquot and analysed (Figure S1B).

In the second experimental set, EVs were isolated from the pPFP of five other healthy donors (three females, mean age 28.6 years). After the isolation, an aliquot of the sample was freshly analysed (particle concentration and size, contaminant protein concentration, TEM). The samples were then split into two aliquots. One aliquot was destined to snap freeze-thaw cycles, the other to slow freeze-thaw cycles. All samples were analysed before and after each of three cycles of freezing and thawing, separated by 1 week of storage at −80°C (particle concentration and size, contaminant protein concentration, TEM). Immunogold labelling was performed with fresh sample and after the first freeze-thaw cycle.

The third experimental set was designed to analyse possible fusion phenomena occurring in the context of storage and freeze-thaw cycles. EVs were isolated by murine microglial cell lines (BV2) genetically modified to express green fluorescent protein (GFP) or mCherry as membrane proteins (see after). Single-positive EVs (GFP^+ and $mCherry^+$) were homogeneously mixed and freshly analysed by flow cytometry. Samples were then analysed after every cycle of freeze (-80°C) and thaw, to check the possible incidence of double-positive EVs after storage as an indication of membrane disruption and lipid re-micellization. TRPS was used to analyse particle concentration and size of three independent preparations of EVs samples for each of the following EVs sources: wild-type (WT) BV2, GFP^+ BV2, $mCherry^+$ BV2. TRPS was performed freshly and after two freeze-thaw cycles.

2.2 | Plasma sample collection and plasma vesicles isolation

Blood samples were drawn by venipuncture into EDTA BD Vacutainer Tubes (BD Bioscience). During blood collection, all the healthy donors were in pre-prandial status. Processing of the samples was started immediately after collection. Blood samples were centrifuged at 3000 x g for 15 min to obtain platelet-poor plasma (PPP) by collecting the supernatant. PPP was subjected to a second centrifugation at 3000 x g for 15 min. The supernatant was collected obtaining platelet-free plasma (PFP) (Jeppesen et al., 2019). PFP was then centrifuged for 40 min at 15000 x g at 4°C to remove cell debris (Jeppesen et al., 2019) obtaining pPFP. The supernatant was then filtered through a 0.22 μm filter (Millipore).

Commercially available qEV size exclusion chromatography (SEC) columns (Izon Science) were used to isolate EVs from filtered pPFP. qEV2 and qEVoriginal, both with a 70 nm pore size, were used for isolation from fresh and stored pPFP, respectively, according to the volume available for the extraction. Following the manufacturer's protocol, after discarding the void volume, the EVs fractions were pooled together for further analysis, obtaining a final volume of 8 mL when using qEV2 and of 1.5 mL with qEVoriginal.

2.3 | Storage conditions

For the first experimental set, the FE samples (suspended in PBS) and the pPFP samples were stored in cryogenic vials (Corning, USA) in eight different conditions, according to the study design. The storage conditions were the following: (A) storage at −80°C without any preservative; (B) Trehalose 25 mM; (C) DMSO 6%; (D) DMSO 10%; (E) Glycerol 30%; (F) Protease Inhibitor Cocktail (Sigma); (G) Sodium Azide 0.02%; (H) Trehalose 25 mM + lyophilization. All conditions except G were stored at −80°C. G condition was stored at +4°C.

For lyophilization, samples were frozen in the presence of trehalose 25 mM and then lyophilized in a vacuum overnight using LIO5P 4K lyophilizator (5pascal). After lyophilization, the samples were stored at −80°C. Before use, lyophilized samples were thawed and rehydrated with PBS to the original volume. Samples were then resuspended immediately before their use.

In the second experimental set, for snap cycles, liquid nitrogen was used to freeze the samples (3 min of sample full immersion in liquid nitrogen) and they were thawed in a 37°C water bath for 5 min. For slow cycles, samples were directly stored at −80°C and thawed on ice until completely liquid. Vesicles were then used immediately after thawing for the dedicated analysis.

2.4 | Particle concentration, size and zeta potential with tunable resistive pulse sensing

Size distribution, concentration and ζ (zeta) potential of isolated EVs were measured by TRPS technology using the qNano instrument (Izon Science Ltd.). The instrument was set according to the manufacturer's instructions for the measurement. For particles measurement, calibration particles CPC100 beads (Izon Science) were used. Samples were diluted in measurement electrolyte (PBS+ 0,3% wetting solution, Izon Science) to achieve a particle flow between 200 and 400 particles per minute. EVs were measured using the NP150 nanopore, with optimal size detection ranging from 50 to 350 nm (Izon Science). Stretch, voltage and pressure were maintained constant between samples and calibration while measuring size and concentration. Instead, while measuring ζ potential, pressure and voltage could be modulated in the range of calibration. Samples were analysed until 500 particles were counted. Flow rate perturbation were excluded from recorded measurements. Data processing and analysis were done on the Izon Control Suite software v3.4. Filter option in the Izon software was used to sort small and large vesicles, setting the filter for small EVs (sEVs) on a measure comprised between 20 and 200 nm, while for large EVs (lEVs) the filter was set between 200 and 800 nm. The Gauss distribution was matched to histograms. Table S1 displays the general settings for TRPS measurement in all samples. Raw data were deposited in Zenodo (https://doi.org/10.5281/zenodo.5258121).

2.5 | Contaminant protein measurement

Contaminant protein concentrations were measured in non-lysed EVs samples using a Pierce Micro BCA Protein Assay Kit (#23235 Thermo Scientific, Pierce Biotechnology) according to manufacturer's protocol.

2.6 | Transmission electron microscopy and immunogold labelling

For EVs samples, formvar carbon copper grids (TEM-FCF100CU, Sigma Aldrich) were deposited on EVs drop for 5 min RT, then the grids were stained with uranyl acetate for 70 s. Samples were analysed via TEM FEI Talos L120C G2 Transmission Electron Microscope.

TABLE 1 List of western blot antibodies

Antibody	Dilution	Code
Alix	1:1000	ABC40 Millipore
ANXA1	1:1000	ab214486 Abcam
Flottilin-1	1:1000	#610820 BD
H3	1:2000	MAB-91904 IS
Lamp1	1:1000	#3243 CS
ApoE	1:1000	Ab183597 Abcam
GM130	1:1000	#610823 BD
GFP	1:2000	A11122 Thermo Fisher
mCherry	1:2000	M1127 Thermo Fisher

For immunogold labelling of fresh EVs, samples were incubated with monoclonal mouse anti-human anti-CD63 antibodies (sc-5275, Santa Cruz biotechnology) for 30 min at RT. Samples were then incubated with EM Grade 20 nm Goat anti-Mouse IgG(H+L) Conjugate (EM GMHL20, BBI solutions) for 30 min, at room temperature (RT). Formvar carbon copper grids (TEM-FCF100CU, Sigma Aldrich) were deposited on EVs drop for 5 min at RT, then grids were stained with uranyl acetate for 70 s. For the immunogold labelling of stored EVs samples, formvar carbon copper grids (TEM-FCF100CU, Sigma Aldrich) were deposited on EVs drop for 5 min at RT, grids were deposited for 10 min RT on drop containing monoclonal mouse anti-human anti-CD63 antibodies (sc-5275, Santa Cruz biotechnology), then briefly washed five times with PBS. Grids were then deposited for 10 min RT on drop containing EM Grade 20 nm Goat anti-Mouse IgG(H+L) Conjugate (EM GMHL20, BBI solutions). Grids were washed briefly five times in PBS and stained with uranyl acetate for 70 s. Samples were analysed via TEM FEI Talos L120C G2 Transmission Electron Microscope.

2.7 | Western blotting

For the protein quantification for WB analysis, EVs samples were lysed in TEN solution with protease inhibitor cocktail (Sigma C3228, P8340), via mechanical homogenization. Protein concentration was measured using a Micro BCA Protein Assay Kit (#23235, Thermo Scientific) according to the manufacturer's protocol. Proteins were stored at −20°C. Quantified proteins were aliquoted and boiled with Laemmli buffer (4% sodium dodecyl sulphate, 20% glycerol, 0.1 mM Tris pH 6.8, and 0.005% of bromophenol blue) for 5 min at 100°C. Samples were resolved in SDS-PAGE gels (10% handmade gels), gels were blotted onto membranes (Amersham™ Protran™, 10600003 GE Healthcare Life Science) via Trans-Blot Turbo Transfer System (Biorad). Membranes were blocked for nonspecific sites with 5% non-fat dry milk in TBS (50 mM Tris-Cl, pH 7.5, 150 mM NaCl) for 1 h at RT, then membranes were incubated overnight (O/N) with primary antibodies in 5% non-fat dry milk TBS-Tween20 0.5%.

Primary antibodies are indicated in Table 1. EVs and non-EVs markers were chosen in agreement with MISEV2018 guidelines (Théry et al., 2018). Membranes were incubated overnight with primary antibodies at 4°C, washed with TBS-Tween (3 × 10 min), and incubated with secondary antibody at RT for 2 h. Secondary antibodies used were: goat anti-mouse IgG HRP (#1706516, Biorad) and goat anti-rabbit IgG HRP (#1076515, Biorad). After washings, Clarity ECL Western Blotting Substrates (Biorad) was used to visualize bands.

2.8 | Cell culture

Murine microglia cell line BV2 (ICLC ATL03001) was cultured in RPMI 1640 (GIBCO, 11875, RPMI-1640) supplemented with 10% fetal bovine serum (FBS) (Gibco), L-glutamine (L-G) (Gibco) 2 mM and penicillin/streptomycin (P/S) 1% (Gibco). For cell passages, cell supernatant was collected (murine microglia cell line BV2 is semi-adherent) and adherent cells were washed once with PBS1X, then cells were detached with trypsin-EDTA 0,25% (GIBCO, 25300054) for 5 min. Suspended and detached cells were pooled together and centrifuged for 10 min at 300 g. Cell pellet was resuspended in RPMI and seeded according to the downstream use. Cells were passaged on Monday, Wednesday, and Friday in 1:10 ratio in T75 Flask (Corning, Life Science 3814), cultured in 18 mL. After thawing, cells were maintained in culture for maximum nine passages (about 3 weeks). Mycoplasma testing was performed once weekly on Mondays.

2.9 | Plasmid and virus generation

#1514 fGFP lentiviral plasmid was kindly donated by professor Luigi Naldini, San Raffaele Scientific Institute. #1514 mCherry-f was generated by cloning mCherry-f of mCherry-Farnesyl-5 (Addgene, #55045) AgeI/SalI in the backbone of #1514 fGFP AgeI/SalI depleted of fGFP.

Lentiviral vectors were used for the generation of lentivirus. Vectors were produced by transient transfection into human kidney 293T cells. A total of 9×10^6 293T cells were seeded in a15cm^2 Petri dish for 24 h prior to transfection in Iscove modified Dulbecco culture medium (Sigma Aldrich, St. Louis, MO, USA) with 10% FBS, 1% P/S and 1% L-G in a 5% CO_2 incubator, and the culture medium was changed 2 h prior to transfection. A total of 59.75μg of plasmid DNA was used for the transfection of one dish: 9μg of the envelope plasmid pM (VSV-G), 12.5μg of packaging plasmid (pMDLg/pRRE), 6.25μg of REV plasmid, and 32 μg of transfer vector plasmid. The precipitate was formed by adding the plasmids to a final volume of 1125 μl of 0.1× TE/dH_2O (2:1) (1× TE is 10 mM Tris [pH 8.0] plus 1 mM EDTA) and adding dropwise 125 μl of 2.5 M $CaCl_2$, mixing well and filtering at 0.22μm. Then 1250 μl of 2× HEPES-buffered saline (281 mM NaCl, 100 mM HEPES, 1.5 mM Na2HPO4 [pH 7.12]) were added dropwise while vortexing to the previous solution and immediately added to the cultures. The medium (16 mL) was replaced after 14–16 h; the conditioned medium was collected after another 30 h, filtered through 0.22-μm-pore-size cellulose acetate filters and ultracentrifuged at 65,000 x g, for 2h, at RT. The viral pellet was resuspended gently in PBS1X and allowed to homogenize at 4°C O/N.

2.10 | Single clone BV2 line generation

BV2 cells were infected at multiplicity of infection (MOI) of 10 with the appropriate lentivirus. Cells were limiting diluted to 1cell/100μL, plated in a 96-multiwell plate and checked under the microscope for single cell per well distribution. Single cell wells were maintained in culture and passaged to obtain a running stable cell line of BV2 fGFP and BV2 mCherry-f, screened by flow cytometry and selected for optimal mean fluorescent intensity (MFI). Farnesylation allows GFP and mCherry to be linked to all cell membranes, including the plasma membrane and the intraluminal membrane of multivesicular bodies, so that the vast majority of EVs produced by these cells are GFP^+ and $mCherry^+$, respectively (Luhtala et al., 2017).

2.11 | Murine microglial EVs isolation and flow cytometry analysis

BV2 WT, BV2 fGFP and BV2 mCherry-f were grown at 37 °C in a humidified 5% CO_2 atmosphere. For EVs isolation, cells were seeded in 10cm^2 Petri for 48h in RPMI supplemented with 10% EVs depleted- FBS, L-glutamine 2 mM and penicillin/streptomycin 1%. The FBS was EV-depleted by ultracentrifugation (Beckman Optima L-90K Ultracentrifuge) at 100,000 × g O/N at 4°C (Type SW32Ti rotor, Beckman Coulter, Brea, CA) and filtered through a 0.22 μm filter before added to the media. Cells were incubated with 1μM phorbol 12-myristate 13-acetate (Sigma Aldrich, St. Louis, MO, USA) for 30 min at 37°C to enhance EVs release (Cocucci et al., 2009; Sidhu et al., 2004). Cell supernatant was collected and cells and tissue debris were eliminated by centrifugation at 300 × g for 10 min at RT and 2000 × g for 20 min at 4°C. Supernatant was filtered through a 5 μm filters and centrifuged at 100,000 x g for 2h at 4°C. EVs pellet was further washed in 1X PBS and centrifuged at 100,000 x g for 4h at 4°C. EVs pellet was resuspended in 1X PBS for flow cytometry analysis. Samples were stored at −80°C. For the triplicate experiments three different cell passages were used. WT EVs were isolated by BV2 WT at passage 6, 7, 8; fGFP EVs were isolated by BV2 fGFP at passage 4.10, 4.11, 4.12; fmCherry EVs were isolated by BV2 fmCherry at passage 3.7, 3.8, 3.9.

For FSC-VSSC settings Megamix-Plus FSC (#7802, BioCytex) were used to set FSC-VSSC for EVs similar events. About 5×10^9 EVs (estimated by TRPS analysis) were stained 1:100 with Isolectin GS-IB4 From Griffonia simplicifolia (IB4) (Nigro et al., 2021; Zappulli et al., 2016), Alexa Fluor 647 Conjugate (I32450) or with 1:100 IB4 blocked by melibiose as staining-specificity control (IB4 was pre-incubated 1:10 with melibiose 0,1 M for 30 min 4°C) (Sigma Aldrich, St. Louis, MO) for 30 min 4°C, as previously described (Ayoub & Salm, 2003). EVs were diluted 1:200 final in1X PBS before analysis with a CytoflexS Flow Cytometer. For all the experiments, controls (unstained EVs, isotype stained EVs, PBS, PBS with IB4, PBS with IB4 and melibiose) and samples were measured for 4 min at a flow rate of 10μL/min. The MIFlowCyt-Ev table (Table S2) is included in the supplementary section. (Welsh et al., 2020) Raw data were deposited in Zenodo (https://doi.org/10.5281/zenodo.5257247).

2.12 | Statistical analysis

Analyses were performed with SPSS statistical 26.0 (IBM SPSS, NY, USA). For EVs paired samples a Friedman test for repeated measures was performed followed by Dunn's procedure for pairwise comparisons. A Kendall's tau-b correlation was run to determine the relationships between particle concentration and size, and contaminant protein concentration in EVs stored samples.

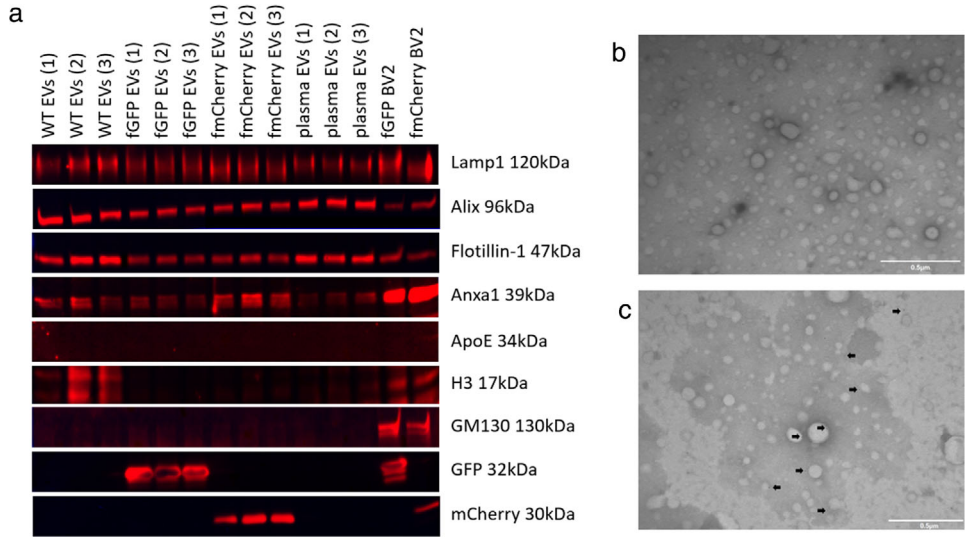

FIGURE 1 EVs characterization: Western blot analysis and TEM imaging – (a) Western Blot probing for vesicular and non-vesicular markers of plasma EVs samples and BV2 samples. As specific EVs associated markers, we used LAMP1, ALIX, Flotillin-1, ANXA1. As non-EVs markers, we used apolipoprotein E (ApoE), histone 3 (H3), GM130. GFP and mCherry proteins marked EVs isolated from fGFP-engineered BV2 and fmCherry-engineered BV2, respectively. BV EVs were isolated by ultracentrifugation from wild-type BV2 (WT EVs), fGFP engineered BV2 (fGFP EVs), and fmCherry engineered BV2 (fmCherry EVs) in three independent preparations. Plasma EVs were isolated with SEC columns as described in methods, from three different healthy donors. fGFP engineered BV2 (fGFP BV2) and fmCherry engineered BV2 (fmCherry BV2) are included as positive controls. (b) Representative TEM images of fresh plasma EVs stained with uranyl acetate. In (c) immunogold labelling performed with anti-CD63 antibody confirmed the EVs nature of the observed particles (c)

General linear models (two-way mixed ANOVA) were performed to assess the effect of time, storage conditions and their interaction on EVs samples.

2.13 | Ethical statement

The study was in agreement with the Declaration of Helsinki and was approved by the San Raffaele Scientific Hospital Ethical Committee. Written informed consents were obtained from all the healthy donor of blood samples.

2.14 | Raw data publication

Raw data are accessible in Zenodo public repository. For FCM data: https://doi.org/10.5281/zenodo.5257247. For TRPS data: https://doi.org/10.5281/zenodo.5258121. We have submitted all relevant data of our experiments to the EV-TRACK knowledgebase (EV-TRACK ID: EV210237) (Van Deun et al., 2017).

3 | RESULTS

3.1 | EVs characterization: Western Blotting and Transmission Electron Microscopy

We performed WB analysis and TEM imaging to determine the presence of EVs in the samples after EVs isolation procedures. WB analysis was performed in agreement with MISEV2018 guidelines (Théry et al., 2018), analysing the presence of well-characterized EVs markers (categories 1 and 2 according to MISEV2018) and non-EVs markers (category 3) (Théry et al., 2018). WB was performed for fresh plasma EVs (FE) samples (three samples from three different healthy donors) and BV2-derived EVs samples (three different preparation for each of the following conditions: BV2 WT, BV2 fGFP and BV2 mCherry-f). BV2 fGFP and mCherry-f cells served as controls. WB analysis confirmed the presence of EVs-markers, such as LAMP1, ALIX, Flotillin-1, and Annexin A1 (ANXA-1) (Jeppesen et al., 2019; Théry et al., 2018) both in FE samples and in BV2-derived EVs samples (Figure 1a). Non-EVs markers, such as Histone H3 (Jeppesen et al., 2019), GM130 (Krishnamachary et al., 2021), and Apolipoprotein E (Krishnamachary et al., 2021) were absent in EVs samples, except for H3 that was measurable in two WT BV2-derived EVs samples (Figure 1a). As expected, ANXA-1 was highly expressed in BV2 cells (McArthur et al., 2010). The analysis also confirmed the expression of GFP and mCherry in engineered BV2 cells and in the corresponding EVs.

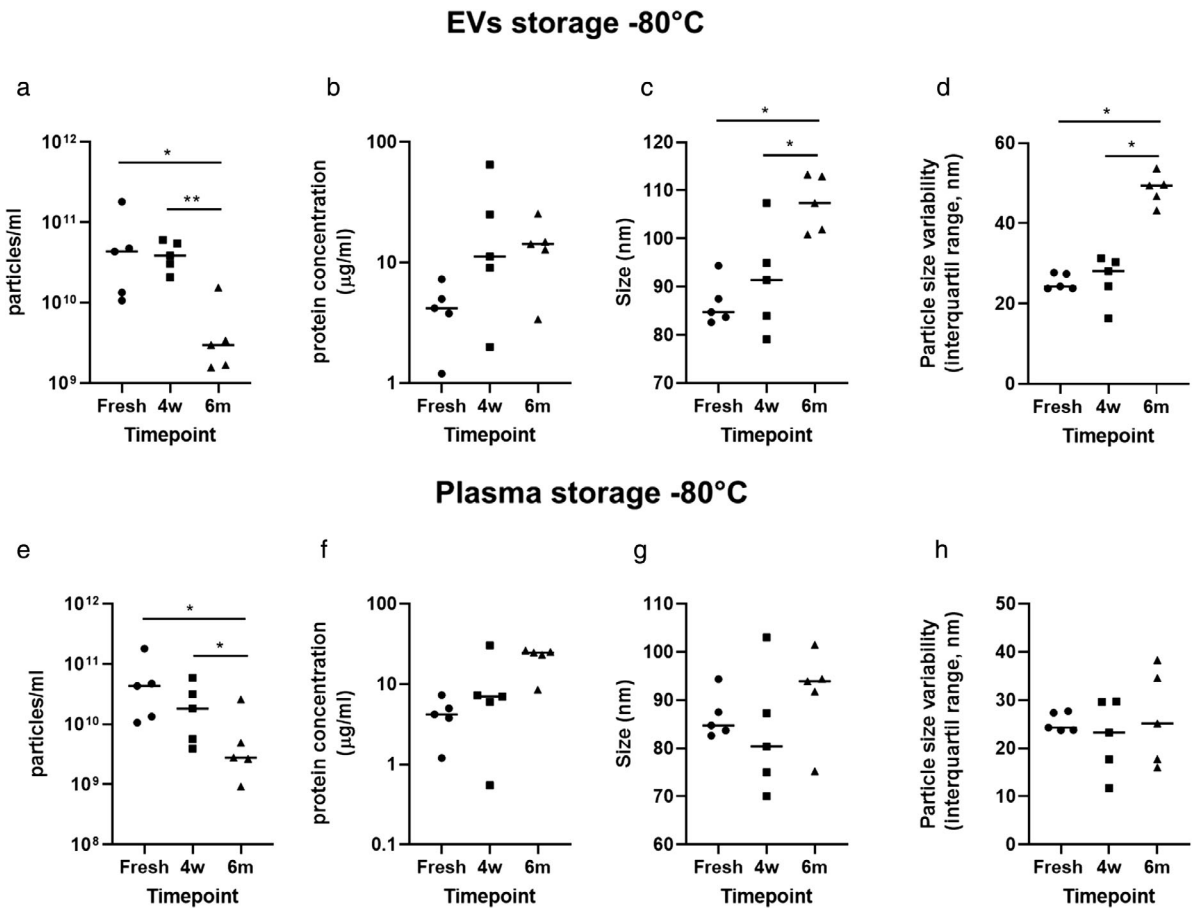

FIGURE 2 Effects of −80°C storage on EVs concentration, size and contaminant protein concentration – Storage reduces EVs yield (a) and EVs recovery from plasma samples (e) in a time-dependent manner. In (b) and (f), the contaminant protein concentration showed a trend to increase over time both in stored fresh EVs samples (b) and when EVs are recovered after plasma storage (f). EVs storage leads to a significant increase in median particle size (c) and size variability (d). On the opposite, the storage of plasma sample did not significantly affect size (g) and particle size variability (h) in EVs recovered after storage. In all figures, significance is expressed as follows: * $P \leq 0.05$, ** $P \leq 0.01$, *** $P \leq 0.001$, **** $P \leq 0.0001$, if not otherwise specified. The test performed is Friedman test followed by Dunn's procedure for pairwise comparisons if not otherwise specified

We performed TEM analyses on FE samples. TEM analysis confirmed the presence of particles with the classical cup-shaped morphology in the range size of EVs (Figure 1b). Immunogold labelling showed that the observed particles were positively stained by the tetraspanin CD63 (Figure 1c), a classical EVs marker (Jeppesen et al., 2019; Théry et al., 2018).

3.2 | Storage affects EVs concentration, sample purity and size

We assessed the effect of −80°C storage on FE and plasma samples on particle yield and contaminant protein concentration. Standard storage at −80°C reduced EVs concentration in a time-dependent manner in stored FE samples ($P = 0.0085$, post-hoc: FE vs. 6 months $P = 0.05$, 4 weeks vs. 6 months $P = 0.0044$; median values, respectively, 4.36×10^{10}, 3.87×10^{10}, 2.99×10^{9}) (Figure 2a).

Similarly, −80°C storage reduced EVs recovery after plasma preservation. ($P = 0.0239$, post-hoc: FE vs. 4 weeks $P = 0.0114$, 4 weeks vs. 6 months $P = 0.0269$; median values, respectively, 4.36×10^{10}, 1.83×10^{10}, 2.79×10^{9}) (Figure 2e).

Contaminant protein concentration showed a time-dependent trend to increase after storage both in FE and pPFP, (in both cases $P = 0.0934$; FE median, respectively, 4.20 μg/mL, 11.25 μg/mL, 14.28 μg/mL; pPFP median, respectively, 4.20 μg/mL, 7.00 μg/mL, 24.72 μg/mL) (Figure 2b, f).

EVs size in FE samples increased over storage time ($P = 0.0239$, post-hoc: fresh vs. 6 months $P = 0.0114$, 4 weeks vs. 6 months $P = 0.0269$. Median size, respectively: 84.77 nm, 91.44 nm, 107.40 nm) (Figure 2c). The storage also increased the spread of size distribution, as demonstrated by a significant increase of the interquartile range (IQR) of size distribution over time ($P = 0.0239$; post-hoc: fresh vs. 6 months $P = 0.0114$, 4 weeks vs. 6 months $P = 0.0269$) (Figure 2d).

On the opposite, median size and variability did not change over storage time in pPFP samples (respectively, $P = 0.37$, $P = 0.69$) (Figure 2g, h).

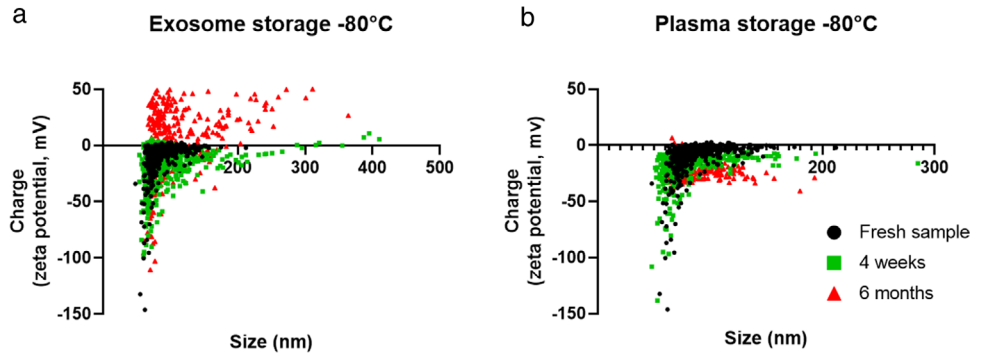

FIGURE 3 Effect of −80°C storage on charge versus size plots – Plots describe the distribution at three different time points of the particles from a single healthy donor as a representative example of the changes occurring during storage. In (a) are shown the changes in stored EVs samples. After 6 months of storage, we observed a shift of the particle population towards positive zeta potential values and increased particle size. The change in distribution was prevented in EVs recovered from stored plasma samples (b)

We run a Kendall's tau-b correlation to determine the relationships occurring among particle concentration and size, and contaminant protein concentration. We found a negative association between particle concentration and particle size ($\tau b = -0.41$, $P = 0.033$) and a positive association between particle size and contaminant protein concentration ($\tau b = 0.371$, $P = 0.05$).

Zeta potential median values did not significantly change over time in FE nor pPFP samples (both $P > 0.9$). In the same direction, no difference in zeta potential variability was found (both $P > 0.5$) (not shown).

Since the TRPS analysis performed allows to measure the zeta potential and the size of a large number of single particles, it is possible to assess the zeta potential values at the particle level. This provides zeta potential data unbiased by particle size distribution that can be expressed as size versus charge plot. The visual inspection of the size versus charge plots revealed that the distribution of zeta potential charges according to particle size markedly changed after storage in FE samples. More in detail, after 6 months of storage, we observed a tendency of particles to have higher individual zeta potential values, with a shift of the particle population towards positive zeta potential values (Figure 3a). The change in distribution was noticeably prevented in plasma stored samples (Figure 3b).

3.3 | Effect of different storage strategies on EVs samples

A general linear model (two-way mixed ANOVA) was performed to detect the effect of storage time and conditions on EVs sample properties, both assessing their independent effect and their interaction. Concerning EVs yield, we found a significant effect of time for all the tested conditions ($F(1.465, 46.890) = 5.945$, $P = 0.01$), with a reduction of concentration after 6 months (post-hoc analysis fresh vs. 6 months $P = 0.001$, 4 weeks vs. 6 months $P = 0.003$, mean values: fresh $= 5.929 \times 10^{10}$, 4 weeks $= 6.919 \times 10^{10}$, 6 months $= 1.267 \times 10^{10}$). On the opposite, we found no effect of the different storage strategies ($F(7, 32) = 1.033$, $P = 0.428$). Moreover, the model found no significant interaction between time and storage conditions ($F(10.257, 46.89) = 0.69$, $P = 0.724$) (Figure 4). In other words, none of the tested strategies was able to interact with time preventing its effect on EVs concentration.

Similarly, for all the conditions, we found a significant effect of time on protein concentration ($F(1.08, 29.611) = 18.853$, $P < 0.0005$; post-hoc: Fresh vs. 4 weeks $P < 0.0005$, fresh vs. 6 months $P < 0.0005$) (Figure S2A) and particle size ($F(1.641, 52.509) = 9.144$, $P = 0.001$; post-hoc: fresh vs. 6 months $P = 0.001$, 4 weeks vs. 6 months $P < 0.0005$) (Figure S2B). We observed no significant effect of storage conditions both for protein concentration ($F(6, 28) = 0.701$, $P = 0.651$) (Figure S2A) and particle size ($F(7, 32) = 0.322$, $P = 0.938$) (Figure S2B). In this case also, we found no significant interaction between time and storage conditions for protein concentration ($F(6.345, 29.611) = 0.8$, $P = 0.0893$) and particle size ($F(11.846, 52.509) = 0.65$, $P = 0.783$).

When we assessed the impact of the different storage strategies on the recovery of EVs from stored plasma samples, we found similar results (Figure S3).

Finally, none of the storage conditions prevented the change in size versus charge plots observed over time in EVs samples (Figure S4)

3.4 | Freeze-thaw cycles reduce EVs yield and increase particle size

We assessed the effect of snap and slow freeze-thaw cycles in terms of EVs concentration, size and contaminant protein. As shown in Figure 5a, a single snap freeze-thaw cycle determined a significant reduction in particle yield. The following cycles did not lead to a further decrease in EVs load ($P = 0.0003$, in post hoc: fresh vs. cycle 1, fresh vs. cycle 2 and fresh vs. cycle 3 $P = 0.001$).

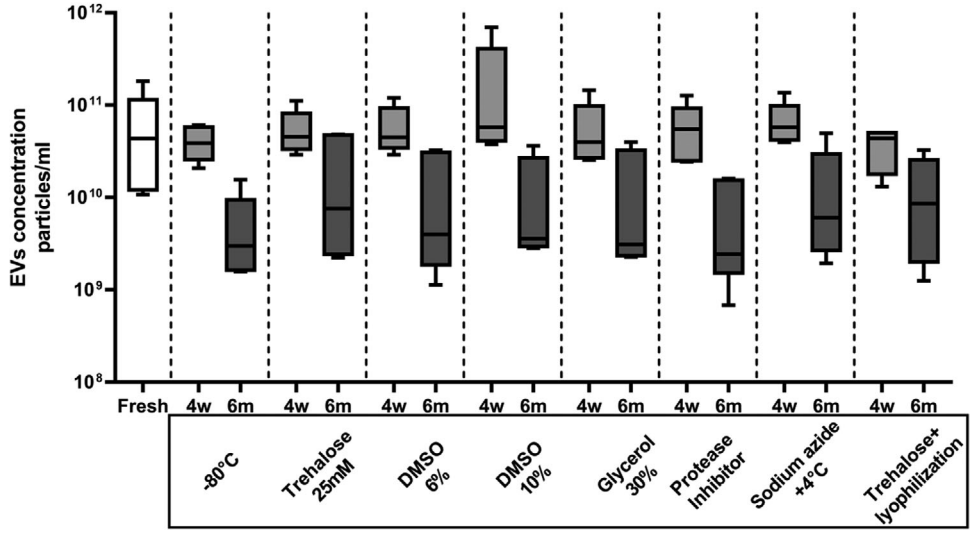

FIGURE 4 Effect of different storage strategies on EVs samples – A time-dependent significant reduction in EVs yield was observed regardless the tested storage strategies (two-way mixed ANOVA). The overall effect of time was significant for all the tested conditions, with a reduction of concentration after 6 months (post-hoc analysis fresh vs. 6 months $P = 0.001$, 4 weeks vs. 6 months $P = 0.003$). No difference has been found among different conditions nor significant interaction between time and storage condition. Significant differences are expressed as *** $P \leq 0.001$ for fresh versus 6 months samples and as ## $P \leq 0.01$ for 4 weeks vs. 6 months

We obtained similar results for slow freeze-thaw cycles ($P = 0.003$, post hoc: fresh vs. cycle 1, fresh vs. cycle 2 and fresh vs. cycle 3 $P = 0.001$) (Figure 5a). We found no differences between slow and snap cycles.

Both snap and slow freeze-thaw cycle led to a progressive increase in particle size, in a cycle-dependent manner, as shown in Figure 5b (snap cycles: $P = 0.0002$, post hoc: fresh vs. cycle 1 $P = 0.025$, fresh vs. cycle 2 $P = 0.0092$, fresh vs. cycle 3 $P < 0.0001$, cycle 1 vs. cycle 3 $P = 0.0106$, cycle 2 vs. cycle 3 $P = 0.025$; slow cycles: cycle: $P < 0.0001$, post hoc: fresh vs. cycle 1 $P = 0.0169$, fresh vs. cycle 2 $P = 0.0028$, fresh vs. cycle 3 $P < 0.0001$, cycle 1 vs. cycle 3 $P = 0.0064$, cycle 2 vs. cycle 3 $P = 0.0346$), without differences between snap and slow cycles.

On the opposite, the protein concentration did not increase in any of the freezing-thawing conditions in the first two cycles (snap $P = 0.69$, slow $P > 0.95$) (not shown).

TEM analysis performed before and after each of the freeze-thaw cycle confirmed a marked reduction of EVs yield, especially after the first freeze-thaw procedure, along with a diffuse increase in particle size (Figure 5c). We observed no differences in TEM imaging between snap and slow freeze-thaw cycles. Immunogold labelling confirmed the presence of CD63-labeled EVs with increased size after the freeze-thaw procedure as compared to fresh samples (Figure 5d).

3.5 | Freeze-thaw cycles induce membrane disruption and re-micellization phenomena

The effects of freeze-thaw cycles on membrane integrity were assessed by flow cytometry. We hypothesized that mixing single-coloured EVs (fGFP and fmCherry) by fluorescent tag linked to the membrane by farnesylation (Luhtala et al., 2017) and analysing the incidence of double-positive EVs after freeze-thaw cycles could indicate membrane disruption and lipid re-micellization. First, we established two engineered single-cell-derived lines expressing fGFP or fmCherry and analysed stable infection and protein production by flow cytometry analysis, checking for stable MFI after several cell passages (Figure S5). We set experiment parameters and acquisition settings as described in MIFlowCyt-EVs Table S2. We assessed a series of negative controls such as PBS (Figure S6A), PBS stained with 1:100 IB4 (Figure S6B), and the respective staining-specificity control with melibiose (Figure S6C). As explained in the material section, melibiose binds with high affinity to IB4, impeding non-specific binding of the IB4 lectin (Ayoub & Salm, 2003). Thus, IB4 gating for $IB4^+$ EVs is localized where vesicles are stained only when stained by IB4, while particles stained by IB4 in the presence of melibiose are excluded by the gating, since they represent non-specific staining (Figure S7). We also included in the supplementary material samples treated with detergent (TritonX100 0,5%) before acquisition in order to lyse vesicles (Figure S8). According to MISEV2018 indications, we also performed and analysed serial dilution measurement of fluorescent EVs to set the proper dilution of vesicles to acquire, setting flow and concentration to avoid the swarm effect (Figures S9 and S10).

In Figure S11, the flow cytometry gating strategy is shown with VSSC-FSC and fluorescence gating. First, BV2-derived EVs were distinguished by Violet-SSC gating and IB4 positive staining. In the last column, the fluorescence of $IB4^+$ events was assessed

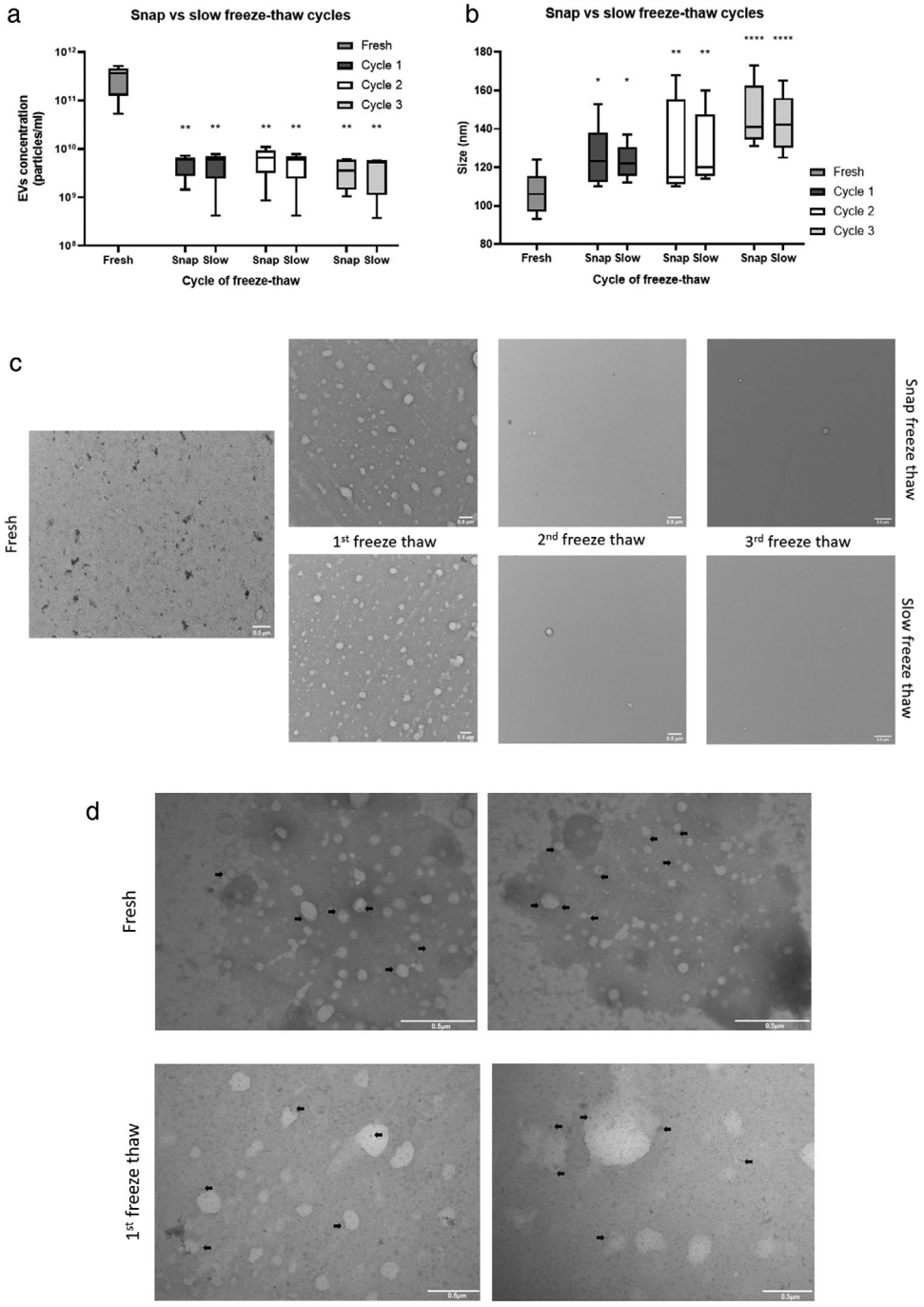

FIGURE 5 Effect of freeze-thaw cycles on EVs samples – Both snap and slow freeze-thaw cycles led to a significant reduction in particle yield after cycle 1 (a) and to a cycle-dependent increase in particle size (b) (Significance is referred to comparisons with fresh samples; no difference was found according to the cycle velocity). EVs preservation through freeze-thaw cycles was also assessed with TEM imaging. In (c) representative TEM images of EVs samples, analysed freshly and after each of three freeze-thaw cycles. Freeze-thaw cycles induced an important reduction of particle yield compared to fresh samples, with no differences observed between snap and slow cycles. In (d) representative immunogold labelling of EVs sample analysed freshly and after a freeze-thaw cycle. EVs were probed by immunogold with CD63 specific antibody and 20 nm gold-conjugated secondary antibody. Black arrows point to CD63 specific labelling on EVs structures. After the freeze-thaw procedure, we observed an increased size of the CD63 labelled particles

and each experiment was checked for non-coloured EVs, fGFP$^+$ EVs, mCherry-f$^+$ EVs and fGFP$^+$mCherry-f$^+$ double positive EVs (mix). In Figure S12, the triplicate experiments and the double-positive population over freeze-thaw cycles are displayed. A table (Table S3) summarizing IB4$^+$ events (number and percentage on parent population) and GFP/mCherry fluorescent events (number and percentage on parent population) was included in the supplementary material. When comparing VSSC-FSC data of IB4$^+$ events before and after freeze-thaw cycles, without finding significant depending on cycles (data in Table S4). For each

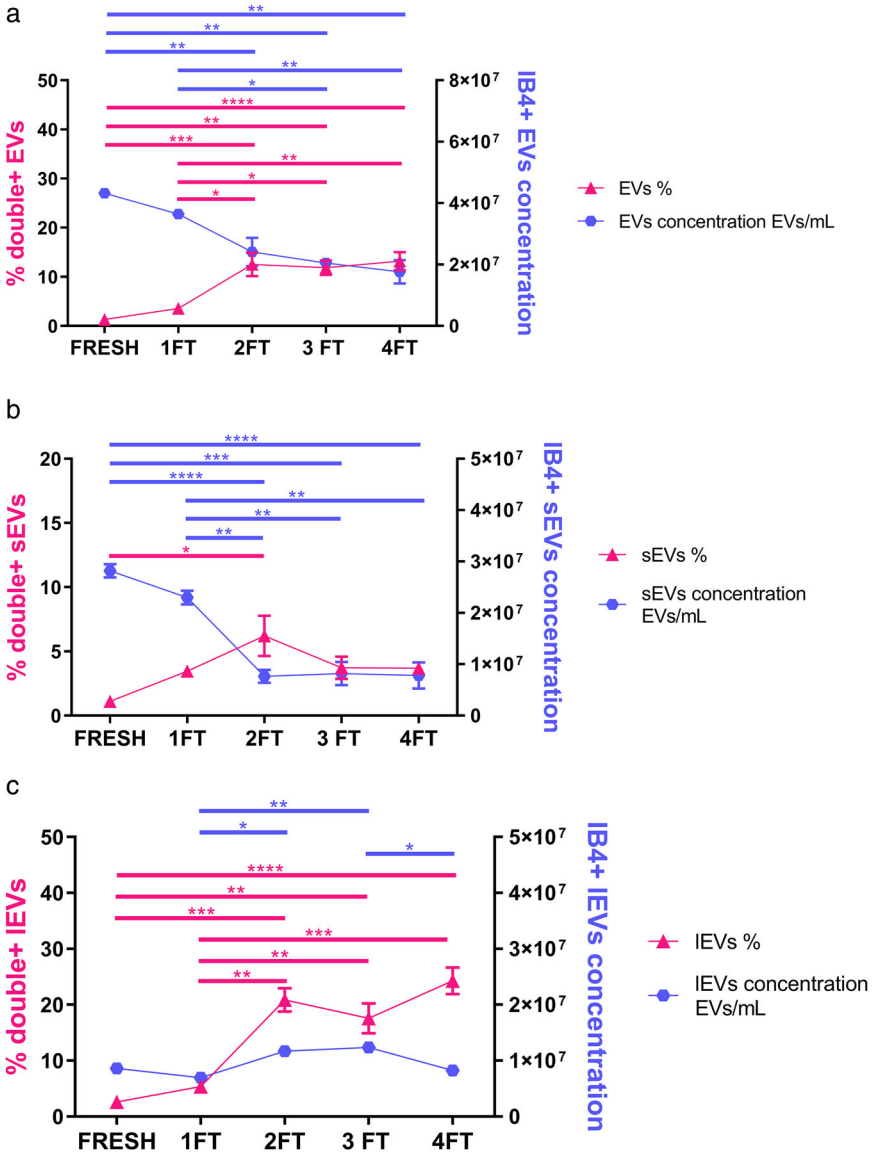

FIGURE 6 Storage leads to EVs disruption and fusion phenomena – In (a) flow cytometer analysis of the whole EVs population (a mix of GFP$^+$ and mCherry$^+$ single positive particles) before and after freeze-thaw cycles. Freeze-thaw cycles induce a reduction in particle concentration (total IB4$^+$ events) and an increased percentage of double-positive EVs (GFP-mCherry$^+$ events). In sEVs subpopulation (b), we observed a marked reduction EVs concentration mostly occurring after the first two freeze-thaw cycles. The percentage of double-positive events showed only a slight increase In lEVs subpopulation (c), freeze-thaw cycles induce a fluctuation of the number of IB4+ events and a marked increase in double-positive events comparing fresh and first cycle samples to subsequent freeze-thaw cycles.

experiment, analysis was performed both on the total EVs population (Figures S11 and S12) and separately on small EVs (sEVs) and large EVs (lEVs) subpopulations (Fig S13). Consistently with MISEV2018 indications, we defined sEVs and lEVs as < 200 nm and > 200 nm, respectively (Théry et al., 2018).

As shown in Figure 6, freeze-thaw cycles determined a significant reduction of IB4$^+$ events recorded at every cycle ($P = 0.006$, see Figure 6a for post-hoc analysis), consistently with the reduction measured with TRPS in the previous experiments. Furthermore, we observed an increased amount of double-positive GFP-mCherry events from basal to > 10% of IB4$^+$ events ($P = 0.0005$). We then separately analysed sEVs and lEVs, finding different results in the two subpopulations.

Taking into account sEVs subpopulation, we observed a significantly marked reduction of IB4$^+$ events mostly occurring after the first two freeze-thaw cycles ($P < 0.0001$, post-hoc analysis in Figure 6b), while the percentage of double-positive events showed only a slight increase ($P = 0.0376$, in post-hoc analysis fresh vs. second cycle $P = 0.045$) (Figure 6b). When considering lEVs subpopulation, we observed a fluctuation of the number of IB4$^+$ events according to the number of freeze-thaw cycles ($P = 0.0047$) (Figure 6c) and a marked increase in double-positive events comparing fresh and first cycle samples to subsequent freeze-thaw cycles ($P < 0.0001$, for post-hoc analysis, see Figure 6c). We then analysed the percentage of lEVs on the total EVs population, separately considering all IB4$^+$ events, the two single-positive populations, and the double-positive population (Table 2). We observed a significant increase in the percentage of lEVs over freeze-thaw cycles in all EVs populations (statistical analysis in Table 2). Interestingly, we found the highest percentage of lEVs when considering double-positive EVs, with lEVs accounting for 87.35% (±3.75%) of the total double-positive events after the fourth freeze-thaw cycle.

We then performed TRPS analysis on EVs samples before and after each of the two freeze-thaw cycles, considering the overall EVs population and sEVs, and lEVs subpopulations (Figure 7). In the overall EVs population, TRPS confirmed a

TABLE 2 Large EVs percentages change according to freeze-thaw cycles

	Fresh	First cycle	Second cycle	Third cycle	Fourth cycle	Friedman test	Post-hoc
% of lEVs among $IB4^+$ EVs	23.47±3.3	22.2±3.6	34.45±5.56	61.77±10.4	51.96±14.82	$P = 0.0028$	Fresh versus third $P = 0.0098$ versus fourth $P = 0.02$ First versus third $P = 0.02$ versus fourth $P = 0.039$
% of lEVs among single positive GFP^+ EVs	33.97±5.3	32.19±6.19	56.93±23.22	64.09±6.96	63.65±21.53	$P = 0.015$	Fresh versus third 0.07 First versus second $P = 0.02$ versus third $P = 0.0098$ versus fourth $P = 0.039$
% of lEVs among single positive $mCherry^+$ EVs	23.47±3.35	22.28±3.6	34.45±5.56	61.77±10.4	51.96±14.82	$P = 0.0028$	Fresh versus third $P = 0.0098$ versus fourth $P = 0.02$ First versus third $P = 0.02$ versus fourth $P = 0.039$
% of lEVs among double positive GFP^+ $mCherry^+$ EVs	34.47±22.36	34.00±17.65	87.42±29.42	81.49±45.43	87.35±3.75	$P = 0.0028$	Fresh versus second $P = 0.07$ versus third $P = 0.07$ versus fourth $P = 0.07$ First versus second $P = 0.039$ versus third $P = 0.039$ versus fourth $P = 0.039$

The percentage of lEVs increased in a cycle-dependent manner, following freeze-thaw cycles among $IB4^+$ events, among GFP^+ or $mCherry^+$ single positive EVs and in GFP^+ $mCherry^+$ double positive EVs. The highest percentage of lEVs was observed among double positive EVs. Data are presented as median ± interquartile range. In the table significant post-hoc results and trend towards significance ($P < 0.1$) are shown. Significant results are in bold.

significant reduction of EVs concentration after the second freeze-thaw cycle (Figure 7a, details of the analysis in figure caption). We observed similar results when considering the sEVs subpopulation (Figure 7b). Taking into account lEVs, despite a reduction in median concentration following the first freeze-thaw cycle, the difference was not significant (Overall median values: fresh 3.63×10^{10}; first cycle 1.65×10^{10}; second cycle 1.84×10^{10}) (Figure 7c). In this case also, the percentage of lEVs on the total EVs population significantly increased after the second freeze-thaw cycle both compared to fresh and first cycle (fresh 15.24%, first cycle 14.25%, second cycle 25.48%; $P = 0.013$, post-hoc analysis: fresh vs. second cycle $P = 0.24$, first cycle vs. second cycle $P = 0.014$ Figure 7d). Similarly, to what was observed with plasma-derived EVs, the analysis revealed a cycle-dependent increase in particle size (Figure 7e).

4 | DISCUSSION

In the present study, we addressed the effect of storage on EVs. While ISEV previously provided indications regarding storage strategies (Witwer et al., 2013), more recent guidelines only suggest to clearly specify the storage protocols used for EVs or biological matrix (Théry et al., 2018). In a recent ISEV expert position paper, no consensus has been reached regarding the impact of storage on EVs physical properties and functionality (Russell et al., 2019). Furthermore, ISEV recently stressed the need for further well-designed research regarding storage and EVs stability to decrease the pre-analytical variability of blood-derived samples (Clayton et al., 2019). In the past years, only a few studies were mainly focused on this issue (Jeyaram & Jay, 2018; Kusuma et al., 2018) and most of them analysed the effect of short-term periods of storage (i.e., hours to 4 weeks) (Agrawal et al., 2017; Charoenviriyakul et al., 2018; Cheng et al., 2019; El Baradie et al., 2020; Jeyaram & Jay, 2018; Lee et al., 2016; Lőrincz et al., 2014; Maroto et al., 2017; Park et al., 2018). Studies focused on longer preservation periods (i.e., months to years) mostly assessed the effect on the recovery of EVs from stored biological samples, with partially conflicting results (Ayers et al., 2011; Muller et al., 2014; Welch et al., 2017).

We investigated the long-term effect of −80°C on EVs samples and EVs recovered after plasma storage. We designed a systematic study to compare the performance of eight different storage strategies. We also focused our attention on the effect of freeze-thaw cycles on EVs concentration, size, and membrane integrity.

We demonstrated that −80°C storage leads to a time-dependent decrease in EVs concentration, with a significant reduction in EVs load after 6 months of EVs or plasma storage. Despite different storage times and techniques used in this work, the

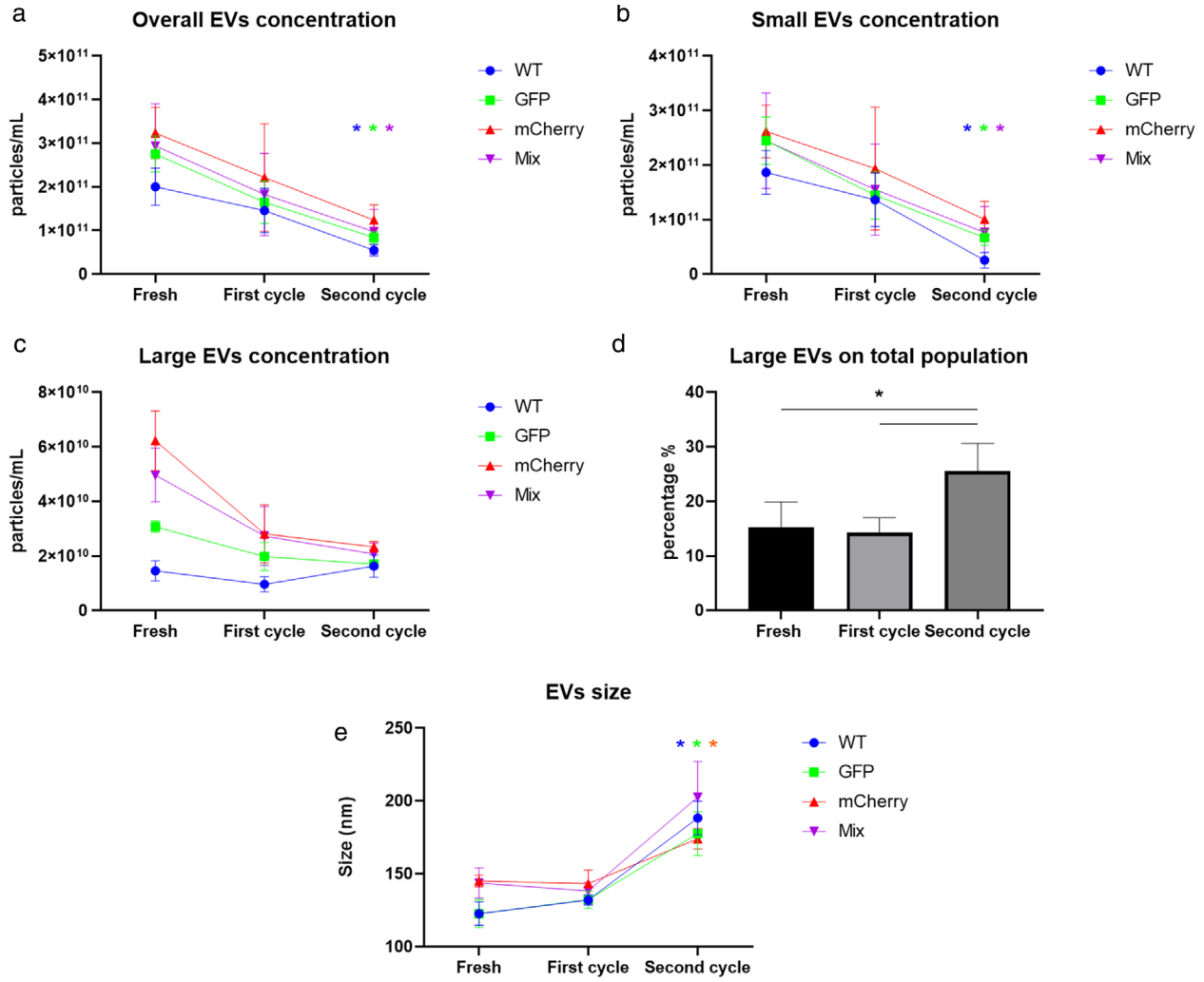

FIGURE 7 TRPS analysis of BV2-derived EVs undergoing freeze-thaw cycles – TRPS analysis showed a reduction in particle concentration in the overall EVs population (a) and in sEVs (b). In (a) Friedman was performed for overall EVs population, resulting significant for wild-type (WT) ($P = 0.028$, post hoc analysis fresh vs. second cycle $P = 0.0143$), GFP ($P = 0.028$, post hoc analysis fresh vs. second cycle $P = 0.0143$) and mixed (GFP and mCherry) BV2-derived EVs ($P = 0.028$, post hoc analysis fresh vs. second cycle $P = 0.0143$) (overall median values: fresh 2.54×10^{11}; first cycle 1.44×10^{11}; second cycle 7.93×10^{10}). In (B) Friedman test performed for sEVs, significant for WT, GFP and mixed population (for all conditions, $P = 0.028$, post hoc analysis fresh vs. second cycle $P = 0.0143$) (overall median values: fresh 2.25×10^{11}; first cycle 1.26×10^{11}; second cycle 5.91×10^{10}). In (c) we found no significant difference in lEVs concentration ($P = 0.36$ for WT, $P = 0.19$ for all other conditions. Overall median values: fresh 3.63×10^{10}; first cycle 1.65×10^{10}; second cycle 1.84×10^{10}). In (D) we observed a significant cycle-dependent increase of the percentage of lEVs on the total EVs population ($P = 0.013$, post-hoc analysis: fresh vs. second cycle $P = 0.24$, first cycle vs. second $P = 0.014$). In (E) EVs size increased after the second freeze-thaw cycle in WT ($P = 0.028$, post hoc analysis fresh vs. second cycle $P = 0.0143$), GFP ($P = 0.028$, post hoc analysis fresh vs. second cycle $P = 0.0143$) and mCherry samples ($P = 0.019$, post hoc analysis fresh vs. second cycle $P = 0.041$) (Overall median values: fresh 139±29 nm, first cycle 134.5±17 nm, second cycle 181±47 nm)

observation of EVs decrease after FE storage is consistent with part of the previous studies (Cheng et al., 2019; Park et al., 2018). On the opposite, other works find no storage-dependent reduction in EVs load, but they have addressed only short-term storage periods (Lee et al., 2016; Lőrincz et al., 2014). Regarding EVs recovery after biological sample storage, our results are consistent with what was previously observed (Ayers et al., 2011; Oosthuyzen et al., 2013). Nevertheless, other authors have found no impact of storage on EVs recovery working with semen (Welch et al., 2017) and urine (Zhou et al., 2006) samples. However, the different techniques used in these works may account for the dissimilar findings observed.

We found that samples analysed after storage were less pure compared to fresh samples in terms of contaminant protein concentration. This is consistent with what was observed by Maroto et al. (Maroto et al., 2017), who found after −80°C storage the presence of 194 proteins that were not initially present in the samples. The authors speculated these proteins to be the result of leakage from EVs, possibly due to particle lysis during storage. This is in line with our observation of an increase in contaminant protein concentration, due to a parallel decrease in particle load and increase in protein concentration. Consistently, Muller et al. (Muller et al., 2014) found a significant increase in contaminant protein after long-term plasma storage.

We also found a time-dependent increase in particle median size in fresh EVs stored at −80°C, negatively associated with the particle concentration reduction and positively associated with the contaminant protein concentration increase, suggesting a relationship among the observed changes. In the same direction, significant change in EVs morphology or size after storage has been observed by different authors and assessed with different techniques. While some studies found a reduction in size after a variable period of storage (Park et al., 2018; Wu et al., 2015), more recent studies found an increase in EVs size over time (Lőrincz et al., 2014; Maroto et al., 2017). When analysing particles recovered from stored plasma, we failed to observe a significant impact of preservation on EVs size and variability.

Differently from Maroto et al. (Maroto et al., 2017) - who observed an increase in the zeta potential of EVs samples after 4 days of −80°C preservation - we found no differences in median zeta potential after storage. However, by measuring zeta potential at single-particle level, in charge-size plots, we observed a tendency of particles to have higher individual zeta potential values after storage, with a shift of the population towards positive values. These changes were not prevented by any of the tested storage strategies. Besides, the changes in charge-size plot distribution over time revealed the impact of −80°C storage on particle population. In other words, EVs population observed after storage seem to have different physical characteristics compared to fresh samples. These changes, occurring at single-particle level, may be not easily detectable with conventional measures (e.g., concentration, dimension, median zeta potential) that necessarily refer to the whole sample. Since zeta potential is a measure that reflects the charge of particles in a certain medium (Midekessa et al., 2020), the possible reasons explaining the changes observed in the present study may be different. Surface charges are, at least in part, sustained by phospholipids composition of EVs membrane and their interaction with membrane proteins (Beit-Yannai et al., 2018; Koog et al., 2021; Midekessa et al., 2020). Thus, one could argue that the possible aggregation/fusion phenomena occurring during storage (and discussed below) may induce a re-arrangement of phospholipid composition or in lipid-protein interactions, leading to changes in zeta potential values. We also observed an increase in contaminant protein concentration. This may lead to a change in medium characteristics not assessed in the present study (e.g., medium pH), but known to modify zeta potential (Midekessa et al., 2020). However, despite the reliability of our observations throughout all the storage strategies tested, it is not possible to exclude their artefactual nature. They may depend on the co-occurrence of EVs disruption with the enrichment of non-EVs components with higher zeta potential in the samples.

Interestingly, in EVs recovered after storing plasma this population shift seems to be at least partially preserved. This finding should be read along with the absence of size and size variability changes observed after plasma storage. Along these lines, one could argue that when preserved in their biological source, EVs may be less exposed to the impact of storage on their physical properties, likely due to a more physiological environment during storage.

We also assessed the impact of multiple freeze-thaw cycles on plasma-derived EVs samples. We observed a significant reduction in EVs load after the first cycle, as measured with TRPS and confirmed with TEM. These findings are in line with what was observed in previous studies (Cheng et al., 2019; Jayachandran et al., 2012; Kim et al., 2005). More in detail, Jayachandran et al. (Jayachandran et al., 2012) and Cheng et al. (Cheng et al., 2019) both found a significant decrease in EVs concentration after the first freeze-thaw cycle. Kim et al. (Kim et al., 2005) demonstrated with electron microscopy membrane disruption occurring after freeze-thaw cycles. Interestingly, Jayachandran et al. (Jayachandran et al., 2012) observed no reduction in particle load when PFP samples underwent freeze-thaw cycles. This finding possibly suggests a protective role of plasma regarding the freeze-thaw impact on EVs, consistently with what was previously argued.

While consistent with these previous studies, the decrease in particle concentration after the first cycle may appear at least partially conflicting with what we observed in the first experimental set. When we analysed the effect of 4 weeks of storage, we found no significant difference in EVs load as compared to fresh samples. The experimental procedures were the same in both experimental sets and we replicated the experiments with different samples, obtaining reproducible results. Along these lines, it is difficult to explain why thawing samples after 1 week leads to a strong reduction in EVs concentration not observable when samples are thawed after 4 weeks. One could argue that the disruption phenomena and re-micellization processes, that we discuss in the following paragraphs, may need different times to occur. Further studies, however, are needed to better clarify this issue.

Contextually with the particle load reduction, we found a cycle-dependent increase in particle size, with a higher dimension observed after every freeze-thaw cycle. We confirmed the observation of increased particle size after freeze-thaw procedures with TEM and immunogold labelling. An increase in particle size after freeze-thaw cycles has been previously demonstrated by Bosch et al. (Bosch et al., 2016). On the opposite, Sokolova et al. observed no differences in size after freeze-thaw cycles, but the freezing temperature was −20°C (Sokolova et al., 2011).

Issman and colleagues using cryogenic-TEM found that slow freezing led to morphological artifacts and EVs breakage that were not induced by snap freezing (Issman et al., 2013). Trummer et al observed a significant reduction in particle load in slow-thawed samples compared to samples thawed at 37°C (Trummer et al., 2009). On the opposite, Lörincz et al found no differences in EVs load nor functional properties according to freezing/thawing velocity (Lőrincz et al., 2014). Considering these studies, we decided to test if freezing and thawing rapidity could have a different impact on EVs. We found no differences between snap and slow cycle protocols since both conditions led to a comparable increase in size and reduction in load. While the results of Trummer are probably inconsistent with ours because of the different detection techniques (Trummer et al., 2009), one could argue that cryogenic-TEM imaging performed by Issman et al. (Issman et al., 2013) was more sensitive than TRPS in detecting

particle changes after slow freezing. Our results, however, are supported not only by TRPS measurement but also by TEM imaging. Consistent with our findings, Maroto et al. found an increase in EVs size independent of whether the samples were thawed slowly or rapidly (Maroto et al., 2017).

One of the most considerable findings of the present study is that freezing EVs at −80°C results in increased size, occurring both in a time-dependent (6 months of storage) and in a freeze-thaw cycle-dependent manner. The finding is consistent both for plasma and BV2-derived EVs, despite different vesicle sources and isolation procedures. Part of the observed dimensional changes is probably related to osmotic phenomena (e.g., particle swelling) (Lőrincz et al., 2014). Previous studies using TEM imaging found particle aggregation occurring after storage preservation (Lee et al., 2016; Maroto et al., 2017) and a storage-induced multilamellar vesicles formation was also observed (Maroto et al., 2017). It is possible to speculate that freezing induces nano- or micro-crystal in particle lipid layer that could be responsible for both membrane disruption and particle fusion (Lee et al., 2016; Lőrincz et al., 2014; Maroto et al., 2017). As stressed by Maroto et al., according to the affinity between exosomes and liposomes, part of the knowledge regarding these latter particles behaviour is relevant to exosome behaviour (Maroto et al., 2017). In this direction, freeze-thaw cycles have been applied for membrane fusion of multi-lamellar into larger uni-lamellar liposomes, suggesting a role of temporary formation of ice crystals in membrane disruption (Costa et al., 2014; Sato et al., 2016). Besides, a recent work by Sato et al obtained hybrid exosomes fused with liposomes using a freeze-thaw method (Sato et al., 2016). In the present study, EVs load reduction, particle size increase, and increased protein in EVs medium co-occurred. Since we found that the EVs size negatively correlates with EVs reduction and positively with contaminant protein increase, we think these observations should be read together. It is possible to speculate that EVs disruption (supported by concentration decrease and protein increase) plays a role in the subsequent particle aggregation and/or fusion phenomena (suggested by the increased size of particles).

In order to explore the occurrence of membrane fusion phenomena, we designed an experimental set with fluorescent EVs, using pure GFP-EVs and pure mCherry-EVs populations. GFP and mCherry fluorescent markers were designed to intercalate in the phospholipid layer through farnesylation modification. The flow cytometry analysis of freshly mixed populations detected an extremely low level of double-positive EVs. After the storage of this mixed population, we observed a progressive increase in the number and percentage of events displaying both fluorescent signals. We also analysed the differences in EVs concentration and the incidence of double-positive events in the two different subpopulations of sEVs and lEVs. The increased percentage of double-positive particles observed in the whole EVs population appears to be mostly sustained by double-positive lEVs. It may be partially related to the lower sensitivity of flow cytometry in detecting sEVs that could have, at least in part, biased the analysis. This result, however, should be read along with the marked reduction of sEVs and the substantially stable concentration of lEVs over time, measured with flow cytometry. TRPS experiments were consistent with flow cytometry findings. We observed a reduction in the concentration of the overall EVs and sEVs populations with no significant change concerning lEVs. The percentage of lEVs on the total EVs, however, increased after the second freeze-thaw cycle. This is consistent with the marked increase of lEVs percentage observed with flow cytometry especially in the double-positive population. In other words, while we failed to demonstrate an increase in lEVs absolute count, we observed that large particles were more represented in EVs populations after freeze-thaw cycles, both in TRPS and flow cytometry experiments. In the same direction, we found an increase in EVs median size, consistently with all the experimental sets of the present study. Against this background, one could argue that both sEVs and lEVs undergo disruptive processes and that the re-micellization/aggregation phenomena preferentially lead to artefactual larger particles. We speculate that the balance between disruption and fusion/aggregation phenomena may account for the substantially stable lEVs count.

The presence of events with a double-positive signal is possibly related to a process of membrane disruption due to the freezing procedure, followed by a re-micellization of the disrupted membranes into new particles, as occurs during the preparation of chemically synthesized liposomes (Costa et al., 2014; Sato et al., 2016). This hypothesis, however, should be read in the context of technical limitations. TRPS cannot confirm the vesicular nature of the larger particles observed after storage and flow cytometry does not rule out EVs aggregation instead of fusion phenomena. Furthermore, despite technical precautions, it is not possible to completely exclude a swarm effect as responsible for an artefactual nature of the double-positive events. TEM imaging, however, confirmed the presence of larger particles after storage and anti-CD63 immunogold labelling confirmed their vesicular nature. This finding, in the absence of vesicles aggregation in the imaged samples, may suggest the hypothesis of fusion phenomena to be more likely. In addition, the analysis performed with flow cytometry may underestimate the fusion phenomena, allowing to detect only part of the re-micellization processes. When two differently labelled EVs disrupt and then fuse, the different fluorescence is measurable as a double-positive event. On the opposite, when different EVs with the same labelling fuse, it is not possible to detect the new event as artefactual.

If the hypothesis of fusion phenomena occurring during storage holds true, it means that when analysing previously stored EVs we are observing an important number of artefactual particles, with a content that is probably the result of a random collection of proteins and other molecules present in the preserving medium.

As previously discussed, we also found a tendency of single particles to have higher zeta potential values after storage. Firstly, it speaks for a significant impact of storage on EVs physical properties. Zeta potential is a marker of colloidal stability of EVs (Midekessa et al., 2020; Qin et al., 2020), reflects particle surface charge, and affects particle-particle interactions according to

electrostatic repulsion (Beit-Yannai et al., 2018). Zeta potential with absolute values greater than 20–30 mV is thought to warrant colloidal stability (Beit-Yannai et al., 2018; Bosch et al., 2016). The shift in individual particle surface charges observed in our study, with an increased number of particles with positive zeta potential values, could at least partially explain the tendency to particle aggregation/fusion discussed above.

Having observed the changes occurring in stored samples, we carried out a systematic comparison of different storage strategies in the attempt to prevent the effect of storage on EVs. In previous studies, different storage conditions have been tested and compared to the simple freezing of fresh samples. Some authors focused their studies on cryoprotective agents such as DMSO (Tegegn et al., 2016; Wu et al., 2015), trehalose (Bosch et al., 2016), or lyophilization in the presence of trehalose (Charoenviriyakul et al., 2018). Other found beneficial effect of storing samples with protease inhibitors (Zhou et al., 2006). In the present study, we tested all these conditions plus storage with glycerol, another well-known cryoprotective agent, and a +4°C storage condition in the presence of sodium azide as a preservative. None of the tested storage strategies outperformed the −80°C storage condition. The overall effect of the tested strategies was negligible in preventing the impact of storage on samples. A recent study assessed the effect of lyophilization on EVs in terms of particle size and concentration, comparing the impact of lyophilization alone and with the use of different concentrations of trehalose and polyvinylpyrrolidone 40 (PVP40), storing the samples at room temperature (El Baradie et al., 2020). The authors observed better preservation of EVs when using both the cryoprotective agents. The lack of freeze-thaw procedures, along with the use of PVP40, may account for the positive effect observed on stored samples, possibly leading to reduced particle membrane damage. The short-time storage period analysed in this work (i.e., hours), however, prevents a possible comparison with our results.

The limitations of the present study include the possible technical variability of TRPS size and concentration measurements. While a recent paper showed a coefficient of variance (CV) ranging from 1.1 to 1.9% for plasma EVs among different TRPS measures of the same samples (Vogel et al., 2021), higher variability has been reported for size assessment, with CV ranging 2.8-15.6% for median EVs size, depending on qNano technical settings (Coumans et al., 2014). The use of experimental replicates and the consistency of our results throughout all the experimental sets, however, makes the contribution of technical variability to our findings less likely. Other technical issues are the lower EVs detection limit of 70–100 nm (Van Der Pol et al., 2014) along with the lower sensitivity of flow cytometry for sEVs that may have partially biased the study. Another limitation is not having tested EVs functionality. While it is reasonable that the particle fusion/aggregation phenomena supposed may lead to altered particles functionality, future studies are needed to assess this crucial topic.

Taken together, our results show a remarkable effect of −80°C storage and freeze-thaw cycles on EVs samples, with likely marked implications for EVs functionality. The finding of a significant level of particle fusion phenomena suggests a strong remodelling of the samples, with the generation of copious artifacts. We found no storage condition able to prevent or mitigate the impact of storage on EVs.

The urgency for valuable storage strategies comes from the opportunity to simultaneously analyse samples from different sources or patients (Witwer et al., 2013). It could also allow working on previously-biobanked samples (Witwer et al., 2013). This stresses the need for further studies to improve storage techniques and reduce pre-analytical variability in EVs studies. At present, however, we think it should be advisable to work with fresh samples. When storage is strictly needed, following our observations it is possible to suggest a short −80°C preservation time and the storage of biological matrix instead of the isolated EVs sample. Finally, our findings stress the need to take into account the storage condition (if storage is present) when comparing different EVs studies and data.

ACKNOWLEDGEMENTS

Italian Ministry of Health # RCR-2019-23669119_004

The authors thanks Prof. Marco Biggiogera for sharing protocols and labelling techniques for EVs in TEM analysis.

The authors thank Dr. Maria Carla Panzieri and ALEMBIC, an advanced microscopy laboratory established by IRCCS Ospedale San Raffaele and Università Vita-Salute San Raffaele, for the contribution in electron microscopy study.

The authors thank Dr.Valeria Mannella for the support with lyophilization protocols and SCUALI for the fruitful discussion.

DECLARATION OF INTEREST STATEMENT

Gelibter S, Marostica G, Mandelli A, Siciliani S, Podini P, Finardi A report no disclosures. Furlan R received honoraria for serving on scientifc advisory boards or as a speaker from Biogen, Novartis, Roche, Merck, and funding for research from Merck.

ORCID

Stefano Gelibter https://orcid.org/0000-0001-7388-4124

REFERENCES

Agrawal, A. K., Aqil, F., Jeyabalan, J., Spencer, W. A., Beck, J., Gachuki, B. W., Alhakeem, S. S., Oben, K., Munagala, R., Bondada, S., & Gupta, R. C. (2017).Milk-derived exosomes for oral delivery of paclitaxel. *Nanomedicine: Nanotechnology, Biology and Medicine*, *13*(5), 1627–1636.

Ayers, L., Kohler, M., Harrison, P., Sargent, I., Dragovic, R., Schaap, M., Nieuwland, R., Brooks, S. A., & Ferry, B. (2011).Measurement of circulating cell-derived microparticles by flow cytometry: Sources of variability within the assay. *Thrombosis Research*, *127*(4), 370–377.

Ayoub, A. E., & Salm, A. K. (2003).Increased morphological diversity of microglia in the activated hypothalamic supraoptic nucleus. *Journal of Neuroscience*, *23*(21), 7759–7766.

Beit-Yannai, E., Tabak, S., & Stamer, W. D. (2018).Physical exosome:eXosome interactions. *Journal of Cellular and Molecular Medicine*, *22*(3), 2001–2006.

Bosch, S., De Beaurepaire, L., Allard, M., Mosser, M., Heichette, C., Chrétien, D., Jegou, D., & Bach, J. -. M. (2016).Trehalose prevents aggregation of exosomes and cryodamage. *Scientific Reports*, *6*(1), 36162.

Charoenviriyakul, C., Takahashi, Y., Nishikawa, M., & Takakura, Y. (2018).Preservation of exosomes at room temperature using lyophilization. *International Journal of Pharmaceutics*, *553*(1–2), 1–7.

Cheng, Y., Zeng, Q., Han, Q., & Xia, W. (2019).Effect of pH, temperature and freezing-thawing on quantity changes and cellular uptake of exosomes. *Protein Cell*, *10*(4), 295–299.

Clayton, A., Boilard, E., Buzas, E. I., Cheng, L., Falcón-Perez, J. M., Gardiner, C., Gustafson, D., Gualerzi, A., Hendrix, A., Hoffman, A., Jones, J., Lässer, C., Lawson, C., Lenassi, M., Nazarenko, I., O'driscoll, L., Pink, R., Siljander, P. R.-.M., Soekmadji, C.…Nieuwland, R. (2019).Considerations towards a roadmap for collection, handling and storage of blood extracellular vesicles. *Journal of Extracellular Vesicles*, *8*(1), 1647027.

Cocucci, E., Racchetti, G., & Meldolesi, J. (2009).Shedding microvesicles: Artefacts no more. *Trends in Cell Biology*, *19*(2), 43–51.

Costa, A. P., Xu, X., & Burgess, D. J. (2014).Freeze-anneal-thaw cycling of unilamellar liposomes: effect on encapsulation efficiency. *Pharmaceutical Research*, *31*(1), 97–103.

Coumans, F. A. W., Van Der Pol, E., Böing, A. N., Hajji, N., Sturk, G., Van Leeuwen, T. G., & Nieuwland, R. (2014).Reproducible extracellular vesicle size and concentration determination with tunable resistive pulse sensing. *Journal of Extracellular Vesicles*, *3*(1), 25922.

El Baradie, K. B. Y., Nouh, M., & O'Brien, I. I. I. F., Liu, Y., Fulzele, S., Eroglu, A., & Hamrick, M. W. (2020).Freeze-dried extracellular vesicles from adipose-derived stem cells prevent hypoxia-induced muscle cell injury. *Frontiers in Cell and Developmental Biology*, *8*, 181. https://doi.org/10.3389/fcell.2020.00181

Issman, L., Brenner, B., Talmon, Y., & Aharon, A. (2013).Cryogenic transmission electron microscopy nanostructural study of shed microparticles. *Plos One*, *8*(12), e83680.

Jayachandran, M., Miller, V. M., Heit, J. A., & Owen, W. G. (2012).Methodology for isolation, identification and characterization of microvesicles in peripheral blood. *Journal of Immunological Methods*, *375*(1–2), 207–214.

Jeppesen, D. K., Fenix, A. M., Franklin, J. L., Higginbotham, J. N., Zhang, Q., Zimmerman, L. J., Liebler, D. C., Ping, J., Liu, Q., Evans, R., Fissell, W. H., Patton, J. G., Rome, L. H., Burnette, D. T., & Coffey, R. J. (2019).Reassessment of exosome composition. *Cell*, *177*(2), 428–445.e18.

Jeyaram, A., & Jay, S. M. (2018). Preservation and storage stability of extracellular vesicles for therapeutic applications. *The Aaps Journal [Electronic Resource]*, *20*(1):1.

Kim, S. -. H., Lechman, E. R., Bianco, N., Menon, R., Keravala, A., Nash, J., Mi, Z., Watkins, S. C., Gambotto, A., & Robbins, P. D. (2005).Exosomes derived from IL-10-treated dendritic cells can suppress inflammation and collagen-induced arthritis. *Journal of Immunology*, *174*(10), 6440–6448.

Koog, L., Gandek, T. B., & Nagelkerke, A. (2021).Liposomes and extracellular vesicles as drug delivery systems: A comparison of composition, pharmacokinetics, and functionalization. *Advanced Healthcare Materials*, 2100639.

Krishnamachary, B., Cook, C., Kumar, A., Spikes, L., Chalise, P., & Dhillon, N. K. (2021).Extracellular vesicle-mediated endothelial apoptosis and EV-associated proteins correlate with COVID-19 disease severity [Internet]. *Journal of Extracellular Vesicles*, *10*(9), Available from: https://onlinelibrary.wiley.com/doi/10.1002/jev2.12117

Kusuma, G. D., Barabadi, M., Tan, J. L., Morton, D. A. V., Frith, J. E., & Lim, R. (2018).To protect and to preserve: Novel preservation strategies for extracellular vesicles. *Frontiers in Pharmacology*, *9*, 1199.

Lee, M., Ban, J.-J., Im, W., & Kim, M. (2016). Influence of storage condition on exosome recovery. *Biotechnology and Bioprocess Engineering*, *21*(2):299–304.

Lőrincz, Á. M., Timár, C. I., Marosvári, K. A., Veres, D. S., Otrokocsi, L., Kittel, Á., & Ligeti, E. (2014).Effect of storage on physical and functional properties of extracellular vesicles derived from neutrophilic granulocytes. *Journal of Extracellular Vesicles*, *3*(1), 25465.

Luhtala, N., Aslanian, A., Yates, J. R., & Hunter, T. (2017).Secreted glioblastoma nanovesicles contain intracellular signaling proteins and active ras incorporated in a farnesylation-dependent manner. *Journal of Biological Chemistry*, *292*(2), 611–628.

Marostica, G., Gelibter, S., Gironi, M., Nigro, A., & Furlan, R. (2021). Extracellular vesicles in neuroinflammation. *Frontiers in Cell and Developmental Biology*, *8*, 623039. https://doi.org/10.3389/fcell.2020.623039

Maroto, R., Zhao, Y., Jamaluddin, M., Popov, V. L., Wang, H., Kalubowilage, M., Zhang, Y., Luisi, J., Sun, H., Culbertson, C. T., Bossmann, S. H., Motamedi, M., & Brasier, A. R. (2017).Effects of storage temperature on airway exosome integrity for diagnostic and functional analyses. *Journal of Extracellular Vesicles*, *6*(1), 1359478.

McArthur, S., Cristante, E., Paterno, M., Christian, H., Roncaroli, F., Gillies, G. E., & Solito, E. (2010).Annexin A1: A central player in the anti-inflammatory and neuroprotective role of microglia. *Journal of Immunology*, *185*(10), 6317–6328.

Midekessa, G., Godakumara, K., Ord, J., Viil, J., Lättekivi, F., Dissanayake, K., Kopanchuk, S., Rinken, A., Andronowska, A., Bhattacharjee, S., Rinken, T., & Fazeli, A. (2020).Zeta potential of extracellular vesicles: toward understanding the attributes that determine colloidal stability. *ACS Omega*, *5*(27), 16701–16710.

Muller, L., Hong, C. -. S., Stolz, D. B., Watkins, S. C., & Whiteside, T. L. (2014).Isolation of biologically-active exosomes from human plasma. *Journal of Immunological Methods*, *411*:55–65.

Nigro, A., Finardi, A., Ferraro, M. M., Manno, D. E., Quattrini, A., Furlan, R., & Romano, A. (2021).Selective loss of microvesicles is a major issue of the differential centrifugation isolation protocols. *Scientific Reports*, *11*(1), 3589.

Oosthuyzen, W., Sime, N. E. L., Ivy, J. R., Turtle, E. J., Street, J. M., Pound, J., Bath, L. E., Webb, D. J., Gregory, C. D., Bailey, M. A., & Dear, J. W. (2013).Quantification of human urinary exosomes by nanoparticle tracking analysis: Nanoparticle tracking analysis and exosomes. *The Journal of Physiology*, *591*(23), 5833–5842.

Park, S. J., Jeon, H., Yoo, S. -. M., & Lee, M. -. S. (2018). The effect of storage temperature on the biological activity of extracellular vesicles for the complement system. *In Vitro Cellular & Developmental Biology-Animal*, *54*(6), 423–429.

Qin, B., Zhang, Q., Hu, X.-M., Mi, T. -. Y., Yu, H. -. Y., Liu, S. -. S., Zhang, B., Tang, M., Huang, J.-F., & Xiong, K. (2020).How does temperature play a role in the storage of extracellular vesicles? *Journal of Cellular Physiology*, *235*(11), 7663–7680.

Russell, A. E., Sneider, A., Witwer, K. W., Bergese, P., Bhattacharyya, S. N., Cocks, A., Cocucci, E., Erdbrügger, U., Falcon-Perez, J. M., Freeman, D. W., Gallagher, T. M., Hu, S., Huang, Y., Jay, S. M., Kano, S. -. I., Lavieu, G., Leszczynska, A., Llorente, A. M., Lu, Q.…Vader, P. (2019).Biological membranes in EV biogenesis, stability, uptake, and cargo transfer: An ISEV position paper arising from the ISEV membranes and EVs workshop. *Journal of Extracellular Vesicles*, *8*(1), 1684862.

Sato, Y. T., Umezaki, K., Sawada, S., Mukai, S. -. A., Sasaki, Y., Harada, N., Shiku, H., & Akiyoshi, K. (2016). Engineering hybrid exosomes by membrane fusion with liposomes. *Scientific Reports*, *6*(1):21933.

Sidhu, S. S., Mengistab, A. T., Tauscher, A. N., Lavail, J., & Basbaum, C. (2004).The microvesicle as a vehicle for EMMPRIN in tumor–stromal interactions. *Oncogene*, *23*(4), 956–963.

Sokolova, V., Ludwig, A. -. K., Hornung, S., Rotan, O., Horn, P. A., Epple, M., & Giebel, B. (2011).Characterisation of exosomes derived from human cells by nanoparticle tracking analysis and scanning electron microscopy. *Colloids and Surfaces B: Biointerfaces*, *87*(1), 146–150.

Tegegn, T. Z., De Paoli, S. H., Orecna, M., Elhelu, O. K., Woodle, S. A., Tarandovskiy, I. D., Ovanesov, M. V., & Simak, J. (2016).Characterization of procoagulant extracellular vesicles and platelet membrane disintegration in DMSO-cryopreserved platelets. *Journal of Extracellular Vesicles*, *5*(1), 30422.

Théry, C., Witwer, K. W., Aikawa, E., Alcaraz, M. J., Anderson, J. D., Andriantsitohaina, R., Antoniou, A., Arab, T., Archer, F., Atkin-Smith, G. K., Ayre, D. C., Bach, J. -. M., Bachurski, D., Baharvand, H., Balaj, L., Baldacchino, S., Bauer, N. N., Baxter, A. A., Bebawy, M.…Zuba-Surma, E. K. (2018). Minimal information for studies of extracellular vesicles 2018 (MISEV2018): A position statement of the International Society for Extracellular Vesicles and update of the MISEV2014 guidelines. *Journal of Extracellular Vesicles*, *7*(1):1535750.

Trummer, A., De Rop, C., Tiede, A., Ganser, A., & Eisert, R. (2009). Recovery and composition of microparticles after snap-freezing depends on thawing temperature: *Blood Coagulation & Fibrinolysis*, *20*(1), 52–56.

Van Der Pol, E., Coumans, F. A. W., Grootemaat, A. E., Gardiner, C., Sargent, I. L., Harrison, P., Sturk, A., Van Leeuwen, T. G., & Nieuwland, R. (2014).Particle size distribution of exosomes and microvesicles determined by transmission electron microscopy, flow cytometry, nanoparticle tracking analysis, and resistive pulse sensing. *Journal of Thrombosis and Haemostasis*, *12*(7), 1182–1192.

Van Deun, J., Mestdagh, P., Agostinis, P., Akay, Ö., Anand, S., Anckaert, J., Martinez, Z. A., Baetens, T., Beghein, E., Bertier, L., Berx, G., Boere, J., Boukouris, S., Bremer, M., Buschmann, D., Byrd, J. B., Casert, C., Cheng, L., Cmoch, A.…Hendrix, A. (2017).EV-TRACK: Transparent reporting and centralizing knowledge in extracellular vesicle research. *Nature Methods*, *14*(3), 228–232.

Vogel, R., Savage, J., Muzard, J., Della Camera, G., Vella, G., Law, A., Marchioni, M., Mehn, D., Geiss, O., Peacock, B., Aubert, D., Calzolai, L., Caputo, F., & Prina-Mello, A. (2021).Measuring particle concentration of multimodal synthetic reference materials and extracellular vesicles with orthogonal techniques: Who is up to the challenge? [Internet]. *Journal of Extracellular Vesicles*, *10*(3), e12052. https://doi.org/10.1002/jev2.12052

Welch, J. L., Madison, M. N., Margolick, J. B., Galvin, S., Gupta, P., Martínez-Maza, O., Dash, C., & Okeoma, C. M. (2017).Effect of prolonged freezing of semen on exosome recovery and biologic activity. *Scientific Reports*, *7*(1), 45034.

Welsh, J. A., Van Der Pol, E., Arkesteijn, G. J. A., Bremer, M., Brisson, A., Coumans, F., Dignat-George, F., Duggan, E., Ghiran, I., Giebel, B., Görgens, A., Hendrix, A., Lacroix, R., Lannigan, J., Libregts, S. F. W. M., Lozano-Andrés, E., Morales-Kastresana, A., Robert, S., De Rond, L.…Jones, J. C. (2020).MIFlowCyt-EV: A framework for standardized reporting of extracellular vesicle flow cytometry experiments. *Journal of Extracellular Vesicles*, *9*(1), 1713526.

Witwer, K. W., Buzás, E. I., Bemis, L. T., Bora, A., Lässer, C., Lötvall, J., Nolte-'T Hoen, E. N., Piper, M. G., Sivaraman, S., Skog, J., Théry, C., Wauben, M. H., & Hochberg, F. (2013). Standardization of sample collection, isolation and analysis methods in extracellular vesicle research. *Journal of Extracellular Vesicles* *2*(1):20360.

Wu, Y., Deng, W., & Klinke Ii, D. J. (2015).Exosomes: Improved methods to characterize their morphology, RNA content, and surface protein biomarkers. *Analyst*, *140*(19), 6631–6642.

Zappulli, V., Friis, K. P., Fitzpatrick, Z., Maguire, C. A., & Breakefield, X. O. (2016).Extracellular vesicles and intercellular communication within the nervous system. *Journal of Clinical Investigation*, *126*(4), 1198–1207.

Zhou, H., Yuen, P. S. T., Pisitkun, T., Gonzales, P. A., Yasuda, H., Dear, J. W., Gross, P., Knepper, M. A., & Star, R. A. (2006).Collection, storage, preservation, and normalization of human urinary exosomes for biomarker discovery. *Kidney International*, *69*(8), 1471–1476.

SUPPORTING INFORMATION

Additional supporting information may be found in the online version of the article at the publisher's website.

How to cite this article: Gelibter, S., Marostica, G., Mandelli, A., Siciliani, S., Podini, P., Finardi, A., & Furlan, R. (2022). The impact of storage on extracellular vesicles: A systematic study. *Journal of Extracellular Vesicles*, *11,* e12162. https://doi.org/10.1002/jev2.12162